energies

MDPI

Article

Development and Characterization of Concrete/PCM/Diatomite Composites for Thermal Energy Storage in CSP/CST Applications

Adio Miliozzi [1,*], Franco Dominici [2], Mauro Candelori [3], Elisabetta Veca [1], Raffaele Liberatore [1], Daniele Nicolini [1] and Luigi Torre [2]

[1] Italian National Agency for New Technology, Energy and Sustainable Development (ENEA), 00123 Rome, Italy; elisabetta.veca@enea.it (E.V.); raffaele.liberatore@enea.it (R.L.); daniele.nicolini@enea.it (D.N.)
[2] Civil and Environmental Engineering Department, UdR INSTM, University of Perugia, 05100 Terni, Italy; franco.dominici@unipg.it (F.D.); luigi.torre@unipg.it (L.T.)
[3] Calcestruzzi Cipiccia Spa, Strada Maratta 70, 05035 Narni, Italy; mauro.candelori@alice.it
* Correspondence: adio.miliozzi@enea.it

Abstract: Thermal energy storage (TES) systems for concentrated solar power plants are essential for the convenience of renewable energy sources in terms of energy dispatchability, economical aspects and their larger use. TES systems based on the use of concrete have been demonstrated to possess good heat exchange characteristics, wide availability of the heat storage medium and low cost. Therefore, the purpose of this work was the development and characterization of a new concrete-based heat storage material containing a concrete mix capable of operating at medium–high temperatures with improved performance. In this work, a small amount of shape-stabilized phase change material (PCM) was included, thus developing a new material capable of storing energy both as sensible and latent heat. This material was therefore characterized thermally and mechanically and showed increased thermal properties such as stored energy density (up to +7%, with a temperature difference of 100 °C at an average operating temperature of 250 °C) when 5 wt% of PCM was added. By taking advantage of these characteristics, particularly the higher energy density, thermal energy storage systems that are more compact and economically feasible can be built to operate within a temperature range of approximately 150–350 °C with a reduction, compared to a concrete-only based thermal energy storage system, of approximately 7% for the required volume and cost.

Keywords: thermal energy storage; concrete; microencapsulated phase change materials; composites

Citation: Miliozzi, A.; Dominici, F.; Candelori, M.; Veca, E.; Liberatore, R.; Nicolini, D.; Torre, L. Development and Characterization of Concrete/PCM/Diatomite Composites for Thermal Energy Storage in CSP/CST Applications. *Energies* **2021**, *14*, 4410. https://doi.org/10.3390/en14154410

Academic Editor: Sergio Rech

Received: 31 May 2021
Accepted: 16 July 2021
Published: 21 July 2021

1. Introduction

Increasing attention to environmental issues, such as the containment of global warming, reduction of greenhouse gas emissions, environmental sustainability of human activities and the rapid depletion of fossil energy resources [1,2], requires the transition to a different energy system model based on the clean and efficient use of renewable and sustainable energy [3–8] that is also capable of avoiding power grid overloads.

Concentrated solar energy plays an important role in this context because it can provide zero-emission high-temperature heat (CST) and electricity (CSP) [9–12]. The major advantage of CSP/CST plants lies in the possibility to integrate a thermal energy storage (TES) system and therefore store a large amount of solar heat to make it available even in periods when sunlight is not present and to produce electricity at a better cost. This allows the more efficient use of the turbine and other components of the power block.

The basic requirements for a TES system are high stored energy density and compactness, good heat exchange characteristics, wide availability of the heat storage medium (HSM) and low cost [13]. Liquid or solid sensible heat TES is the most commercially used technology. A TES system should be chosen for a particular application based on several considerations, including cost, performance [14] and process integration [15]. Some of the

performance factors of thermal storage systems are their energy capture rate, discharge rate and overall efficiency. Moreover, these factors are strongly influenced by the properties of the HSM, such as specific heat and thermal conductivity. In particular, the stored energy density is an important parameter [16] to evaluate the performance of TES technologies because the required volume should be as low as possible.

This paper is focused on the improvement of the energy density of concrete-based TES. Sensible heat TES (SHTES) systems based on concrete as HSM have been demonstrated to possess many of the abovementioned characteristics to be used as efficient TES. Concrete is a solid HSM characterized by low cost, easy production, good mechanical properties, non-toxicity, non-flammability, good thermal conductivity/diffusivity and the absence of a containment system [17–21]. Its application in this field includes the following technologies: CSP/CST plants, industrial waste heat recovery at elevated temperatures, thermal management of decentralized, combined heat and power systems and other high-temperature processes.

A first concept of concrete based on SHTES was developed and tested by DLR (Germany) at the "Plataforma Solare de Almeria" (Spain) [22]. Concrete was damaged in the start-up phase because, during the heating, water evaporation built up a critical vapor pressure due to the low permeability of the material. A second-generation 20 m^3 solid media storage test module was built and tested in a temperature range between 300 °C and 400 °C by DLR in Stuttgart [23,24]. In this case, a new concrete mix design was developed to optimize the storage capacity, thermal conductivity and vapor permeability of HSM.

From this experience, a new innovative concrete mixture, patented and commercially called Heatcrete, was developed by the NEST company in collaboration with Heidelberg to operate in TES systems for parabolic trough applications at high temperatures up to 393 °C [25]. The DLR concept employs a large pipe register cast into a large block of concrete, while the NEST concept has a new heat exchanger design that uses single thermal elements arranged in series and parallel in a modular frame. Each element comprises a cylindrical, thin-walled (0.4 mm) steel casing, closed at only one end, which contains the Heatcrete concrete with two integrated U-shaped steel pipe heat exchangers. A 1.0 MWh NEST storage pilot was successfully tested in a CSP facility at the Masdar Institute Solar Platform (MISP) in Abu Dhabi, United Arab Emirates, for approximately 6000 h of cycling operation with 279 charge/discharge cycles and showed stable and repetitive performance [26]. However, the thin cylindrical steel casing acted as a permanent casting form. On one hand, it represented the optimum reinforcement and support of the TES element; on the other, it hindered the easy elimination of the free water inside the concrete and, therefore, could be dangerous due to the possible spalling phenomena of the material.

Skinner et al. [27] aimed to incorporate ultra-high-performance concrete (UHPC: compressive strength >150 MPa), which was designed previously, into a TES system capable of storing heat at temperatures up to 500 °C. Results were evaluated and compared based upon the charging time required to elevate the outer surface temperature of the prism from 380 to 430 °C. They adopted solar salts ($NaNO_3$-NO_3 60–40 wt%) as heat transfer fluid (HTF) flowing through a plain pipe and an auger-style, helicoidal fin configuration. Polytetrafluoroethylene (PTFE) and a heat-curing, fibered paste (HCFP) were tested as interface materials to mitigate the stress in the concrete. The authors observed that the fins increased the rate of heat transfer in the concrete, but large cracks formed at each of the fin locations even though the HCFP decreased the number and size of the cracks, albeit not to the desired levels. Guerrero and Collares Pereira [28] incorporated available slag material with a high metallic content from old mines in the area of São Domingos, in the Alentejo region of Southeastern Portugal. Giannuzzi et al. worked on the development of new concrete mixtures and prefabricated modular thermal storage concepts with particular attention paid to increasing the permeability of HSM and therefore its durability [29]. This was possible thanks to a concrete mix with a low water/cement ratio, as well as to the addition of polymeric fibers that facilitated the vapor release at high temperatures, and of metal fibers that increased its thermal diffusivity and mechanical strength [30–32].

The major disadvantage of the use of a concrete-based TES is its low heat stored density [16], which requires the use of large amounts of concrete. A reduction in the concrete's volume and mass can be obtained by increasing the energy stored through the use of a small amount of PCM in the concrete mix design. This allows the storage of energy both as sensible and latent heat, maintaining, at the same time, good mechanical properties. This is the main objective of the research presented in this paper. The incorporation of PCM can be realized by using different methods: direct incorporation, immersion, encapsulation, microencapsulation and shape stabilization [33]. In the direct integration and immersion methods, potential leakage has to be assessed. When the PCM is encapsulated in or added to a shape-stabilized material, the PCM leakage is avoided [34,35]. Shape-stabilized phase change materials (SS-PCM) offer various advantages, including high energy density, good chemical stability and shape stabilization and high mechanical strength [36].

This concrete/SS-PCM-based heat storage solution has already been successfully applied at low temperatures, in the building sector for energy savings, better thermal indoor climate and reduced peak powers [37]. Concrete solutions for TES are usually based on sensible heat transfer and thermal inertia. PCMs incorporated into the concrete wall have been widely investigated to improve building energy performance [38–45]. At low temperatures, organic PCMs such as paraffin or sodium acetate trihydrate (SAT) are normally incorporated into different porous supporting materials, including diatomite [46]), expanded vermiculite [47] and expanded graphite [48]. Due to the microscopic size of the pores of the support materials, this union is identified as a microencapsulated phase change material (mEPCM) [49,50]. Microencapsulation techniques allow the fabrication of advanced PCMs with a greater heat transfer area, reduced reactivity with the outside environment and controlled volume changes during the phase transition. Microcapsules can be described as particles that contain a core material surrounded by a coating or shell and have diameters in the 1–1000 μm range [51].

For medium–high-temperature applications, in the range of 120–1000 °C, an approach similar to the previous one is being evaluated by many researchers. Generally, inorganic PCMs, such as molten salts or their mixtures, such as nitrates, sulfates, chlorides, carbonates and hydroxides, can be used and incorporated into a porous support material, similar to the previous one. They can be considered potential storage media in solar power plants or industrial waste heat recovery systems [14,52]. Unfortunately, there is not much available literature that highlights the performance of concrete including high-temperature mEPCM. Chieruzzi et al. [53] included a small amount of PCM, 2 wt% of solar salts (60% $NaNO_3$-40% KNO_3), with different methods, in a cementitious paste (mortar) composed of type 42.5 Portland cement, 0–4 mm sand and water. These materials were thermally and mechanically characterized after thermal conditioning at temperatures between 25 and 400 °C. The best results were obtained using mEPCM, in which the solar salt was absorbed into the diatomite, a porous carrier structure, with an 80/20 salt/diatomite ratio. This composite showed an increase in thermal conductivity and capacity of approximately 8%. From a mechanical point of view, a relevant increase in flexural strength (+80%) and compression strength (+30%) was registered in comparison with the base mortar. This is a surprising effect, justifiable only through a strong connection between cement and diatomite.

Thus, the purpose of this work was the development and characterization of a new concrete-based heat storage material containing a concrete mix capable of operating at medium–high temperatures (150–400 °C) and with a small amount of mEPCM. The concrete mix was realized to demonstrate the main thermal and mechanical characteristics required for CSP/CST applications [29–32], optimizing the concrete/mEPCM ratio. Additionally, the PCM/diatomite ratio [53] in the mEPCM was analyzed and optimized to reduce the presence of voids and, then, the volume of mEPCM. The same was done for the salt/diatomite ratio, reducing the volume of mPCM itself. This material was characterized both thermally and mechanically, showing promising heat storage properties.

2. Materials and Methods

To develop the new materials, it was necessary to ensure the appropriate amount of microencapsulated PCM (mEPCM or SS-PCM). A new mixture of base concrete had the characteristics mentioned by Miliozzi et al. [29]. The ENEA patent on a new concrete thermal energy storage device was used. Subsequently, it was possible to incorporate a small amount of mEPCM into the base concrete by appropriately replacing some aggregates and creating new mix designs. The study of the concrete mixtures and the realization of the various specimens took place in collaboration with the Cipiccia Calcestruzzi company in Narni (Terni, Italy).

In Figure 1, the methodology adopted is illustrated in a flowchart, highlighting the main steps to develop and characterize the new concrete/mEPCM heat storage materials.

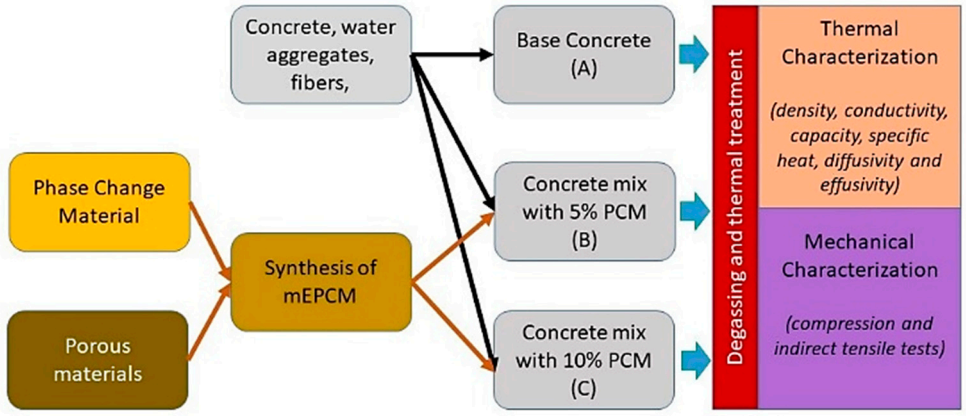

Figure 1. Flowchart of the methodology adopted to develop and characterize new concrete/mEPCM heat storage materials.

2.1. Microencapsulated Phase Change Material

2.1.1. Selection of the PCM for Encapsulation

The choice of the phase change material (PCM) to be used to produce the mEPCM was made based on functionality, energy efficiency and cost-effectiveness criteria. The functionality criteria take into account the chemical and physical characteristics of the PCMs for their use in storage systems. Partially overlapping with the functional characteristics are the energy efficiency criteria, which take into consideration the storage and exchange capacity of thermal energy, expressed in terms of the characteristic properties such as sensible and latent heat, specific heat and thermal capacity. Finally, the evaluation of the costs of the properties described above provides an exclusive criterion for the choice of the PCM mixture to be used. In light of the scientific literature found on PCMs for TES and considering the criteria described, the eutectic mixture of salts, potassium nitrate (KNO_3) and sodium nitrate ($NaNO_3$) was selected. The eutectic mixture (EUT) consisted of (54.3/45.7 wt%) $KNO_3/NaNO_3$, with a melting temperature range between 210 and 240 °C and a maximum peak at approximately 225 °C. The eutectic showed good heat storage capacity, corrosivity and viscosity compatible with use in storage systems for solar plants, as well as low cost [54–59]. The production of the eutectic mixture of salts for the PCM required a preliminary study of the single nitrate salts of potassium and sodium. Samples of approximately 20 mg of each of the nitrate salts, which were previously dried in a vacuum oven for 24 h at 105 °C at 0.2 MPa, were analyzed with a differential scanning calorimeter (DSC) Q200 (TA Instrument, New Castle-DE, US) in a nitrogen inert atmosphere (N_2 flow 50 mL/min). The samples were subjected to 2 heating and cooling cycles between −10 and 360 °C with a temperature ramp of 10 °C/min. In Figure 2, the values of the heat flow concerning the temperature are reported in graphs to allow the analysis of the thermal properties. In Table 1, the transformation enthalpies, melting enthalpy ΔHm and crystallization ΔHc and the temperatures of the main peaks are shown for each thermal cycle.

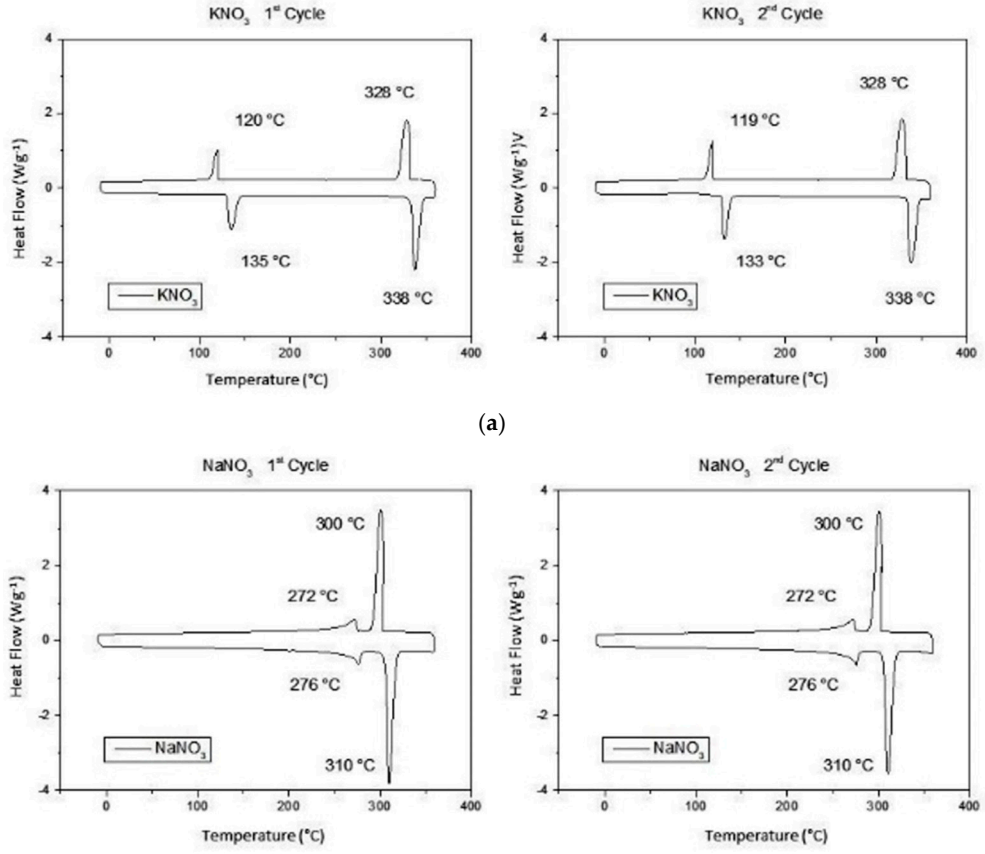

Figure 2. DSC curves of 1st (on the right) and 2nd (on the left) heating/cooling cycles for (**a**) KNO_3 and (**b**) $NaNO_3$. The two curves are related to the heat flow behavior in the temperature range −10 to 360 °C.

Table 1. Calorimetric characteristics by DSC of the basic nitrate salts (transformation enthalpies and temperatures of the main peaks).

Nitrate Salt	1st Heating		1st Cooling		2nd Heating		2nd Cooling	
	ΔH (J/g)							
	ΔHm′	ΔHm″	ΔHc′	ΔHc″	ΔHm′	ΔHm″	ΔHc′	ΔHc″
KNO_3	48.4	92.5	93.7	26.3	46.75	92.0	93.7	26.8
$NaNO_3$	28.1	159.5	160.9	29.4	30.8	159.5	160.3	30.3
	Peak Temperature (°C)							
KNO_3	135.6	337.6	328.7	119.6	132.7	338.4	328.3	119.2
$NaNO_3$	276.2	309.5	300.6	271.8	275.8	310.4	300.6	271.7

The synthesis of the eutectic mixture of $KNO_3/NaNO_3$ in a proportion of 54.3/45.7 wt% was carried out with two different methods: via melt mixing (MeM) and via liquid-assisted compounding (LAC) followed by vacuum drying (VD). The MeM synthesis was carried out by mixing adequate quantities of the two finely powdered salts in a planetary for 30 min at 15 rpm. The mixture was placed in a steel mold oven for 2 h at 360 °C and then slowly cooled for 18 h to room temperature. The LAC + VD synthesis was carried out by heating a solution of 42.87 wt% of deionized water (DIW) to 84 °C and adding 31.03 wt% of potassium nitrate with continuous mixing, and, upon complete dissolution of KNO_3, adding 26.10 wt% of sodium nitrate, mixing until a solution free of salt crystals was obtained. The quantities of salts and solvent for the LAC can be obtained from the solubility graph in Figure 3, where the water used is given by the minimum amount of solvent at 84 °C increased by 25%. Excess water is functional for the impregnation process described below [60].

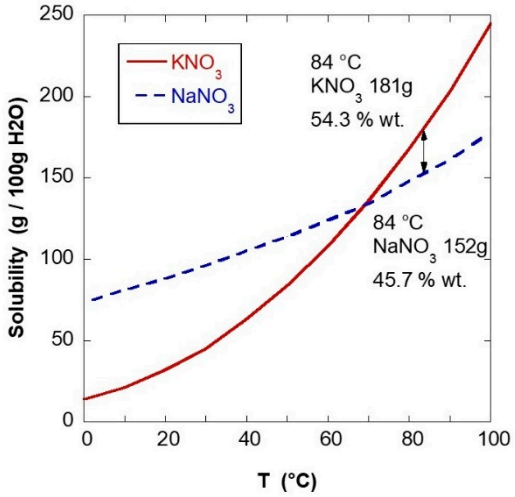

Figure 3. Solubility curves of KNO_3 and $NaNO_3$ concerning temperature per 100 g of water.

The saline solution was quickly dried in a vacuum oven (Vuototest-Mazzali, Lissone, Italy) at 84 °C and 0.2 MPa to limit any selective precipitation of the salts. Since the LAC + VD method offers some important advantages over the MeM method, the mixtures obtained with the two types of synthesis were compared, highlighting the equivalence of the methods on the thermal characteristics of the eutectic. In Figure 4, the comparison of the second heating/cooling cycle in DSC of the salts produced with MeM and with LAC + VD synthesis demonstrates the equivalence of the thermal behavior of the salts.

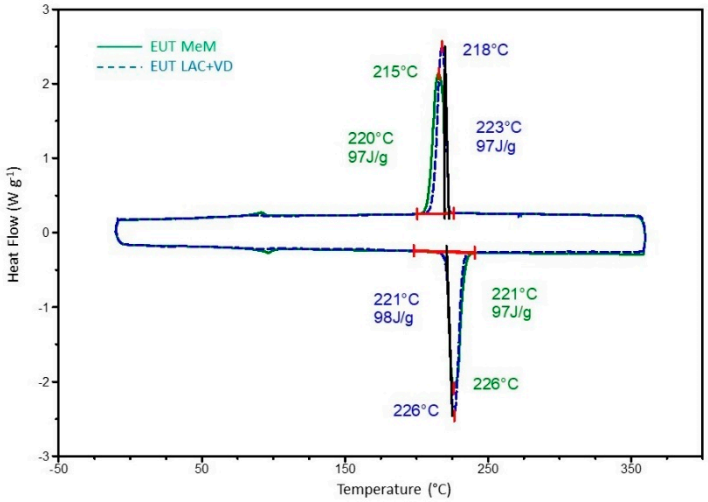

Figure 4. Comparison of DSC curves of the 2nd thermal cycle of eutectic produced with the synthesis in solvent LAC + VD and with the synthesis in melted MeM. The two peak temperatures T_m, T_c and enthalpies ΔHm, ΔHc are presented.

2.1.2. Selection of the Porous Media for Encapsulation

The process of selecting porous media (PM) for encapsulation was carried out in light of extensive bibliographic research and making use of the skills acquired by ENEA and UNIPG researchers during previous studies in this area. The main criteria for the selection were thermal stability, impregnation capacity, compatibility with PCMs, processability in the concrete mix, cost-effectiveness and eco-sustainability of the materials. The thermal stability in the temperature range of the TES application (120–550 °C) is a fundamental requirement for the use of the porous medium for encapsulating the PCM. The impregnation capacity depends on the morphology of the PM and on the method used to insert the PCMs into the cavities. The percentage of impregnation and therefore of PCM content

is crucial for the efficiency of the storage system as the latent heat, which justifies the use of encapsulated PCMs, and must exceed the sensible heat that would be obtained with other materials [53]. Physico-chemical compatibility between PM and PCM is essential concerning the numerous heating and cooling cycles to which the materials in place will be subjected. The processability of the mixture must be considered based on the mixing criteria of the aggregates for the CLS, as the mass production of the TES modules will take place according to the traditional methods of preparation of building materials. Economic factors are unavoidable for a good outcome of the project, especially in consideration of the large quantities required for the use of large plants in TES, so the cost must be competitive. Finally, the eco-sustainability of both raw materials and the entire life cycle of the materials should not be overlooked [61–65]. Based on the criteria taken into consideration, a porous calcined diatomite supplied by DEREF SpA, named DIA2, was selected. DIA2 diatomite is characterized by a density of 0.2 g/cm^3, a sieving residue max 6% by weight at 325 mesh and R.H. max 1% [66].

The behavior of diatomite under thermal degradation was verified with a thermogravimetric analyzer (TGA)—Exstar 6300—by evaluating the TG weight loss as a function of temperature. The tests were performed in a dynamic temperature regime with a 10 °C/min ramp from 30 to 900 °C both in an inert atmosphere (N_2) and air. The results of the thermal degradation tests TG/T and the derivatives (DTG) were calculated and reported in the form of a graph. Figure 5 shows the TG/DTG plot of the selected diatomite.

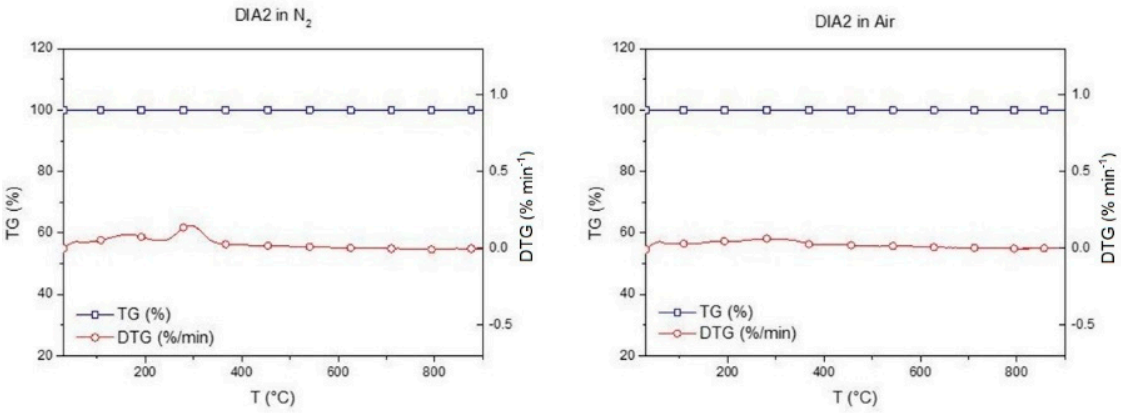

Figure 5. TG/DTG curves of diatomite DIA2 in N_2 and air atmosphere.

DIA2 diatomite, although calcined, shows a very slight weight loss around 293 °C, also attributable to the presence of molecular water [64,67]. Diatomite does not show significant weight loss attributable to thermal degradation, so it is suitable for use as a porous material for PCM encapsulation.

2.1.3. Method of Encapsulation of PCM

In other works, the impregnation was carried out during melting, namely by liquefying the PCMs and mixing them with the porous medium to ensure that the liquid PCM penetrates the PM cavities [68]. Although effective, this method requires high energy expenditure to bring the PCM to fusion, and phenomena involving the release of salts by leakage can occur. A new method of impregnating porous media with PCMs was used, which exploited the advantage offered by the method of synthesis of salts in the solvent. In other studies, it has been found that the impregnation of PCMs in a moist environment is more effective in ensuring a stable encapsulation of the PCMs [69]. The saline solution prepared in LAC was added to the suitably dried porous medium, which rapidly absorbed the salts dissolved in the water. Subsequently, a drying treatment was carried out in a vacuum oven, as described for the synthesis of PCMs. The same synthesis as used for PCM was conducted, but by adding the porous medium. In this way, the production steps were minimized, and energy consumption and the risks associated with

the high temperatures (T > 340 °C) of the melting method were reduced. To maximize the percentage of impregnation, it was decided to operate in depression to minimize the capillary tension inside the cavities of the porous media, both in the absorption phase and in the drying phase. Then, the process was perfected by carrying out the spillage of the saline solution onto the porous medium inside the vacuum oven under a condition of low pressure (0.2 MPa) while maintaining the temperature at 84 °C. A suitable spill tank was built with a mechanism that allowed impregnation operations to be carried out while keeping the oven in depression; the saline solution was gradually poured into the mold, where a layer of the porous medium had previously been deposited, which was impregnated while maintaining a vacuum. Figure 6 shows some phases of the impregnation process.

Figure 6. Impregnation process. (**a**) Vacuum furnace with a movable tank, (**b**) preparation with depressurization, (**c**) spillage of the saline solution onto the porous medium, (**d**) impregnation of the porous medium and (**e**) drying in depression.

The drying was carried out with the same temperature conditions as the impregnation, with pressure oscillating between 0.2 and 0.3 MPa due to saturation by evaporation of the water. As the literature reports a maximum impregnation limit of porous media with a quantity of PCM not exceeding 80 wt%, the DIA2/EUT formulations were produced with 20/80 wt%, in an attempt to increase the efficiency of the mEPCM by 15/85 wt% [53]. The samples obtained were studied by DSC thermal analysis and with a morphological analysis of the fracture surfaces captured with SEM micrographs.

Roughly 20 mg samples of the mEPCMs were subjected to DSC analysis with Calorimeter Q200 performing a thermal cycle of heating from −10 to 360 °C and cooling from 360 to −10 °C twice at a ramp rate of 10 °C/min operating in an inert atmosphere of N_2. The second thermal cycle eliminated the thermal history of the material stored during the synthesis process, allowing a better comparison of the results. The thermal analysis provided characteristic temperatures and transformation enthalpies of the microencapsulated PCMs in both the heating and cooling phases. In particular, during the second heating cycle, the melting (Tm) and crystallization (Tc) temperature and the melting (ΔH_m) and crystallization (ΔHc) enthalpy at the main peak were calculated. The results are summarized in Table 2. The calorimetric parameters of the eutectic mixture EUT of Table 2 show that the temperature of the melting peak in the heating phase was 226 °C and that the variation in melting enthalpy normalized to the mass was 97.7 J/g; during cooling, the temperature of the crystallization peak was set at 218 °C and the enthalpy of solidification was 96.9 J/g. Both peak temperatures and phase change energies were fully within the range of values reported in the literature [70,71].

Table 2. Thermal characteristics of the microencapsulated PCMs obtained by DSC analysis during the 2nd thermal cycle (transformation enthalpies and temperatures of the main peaks).

Name	PM	PCM	Tm	ΔH_m	Ec	Tc	ΔH_c
	wt%	wt%	°C	J/g	%	W/g	J/g °C
EUT	-	100	226	97.7	-	218	96.9
20DIA2	20	80	232	77.9	99.7	211	77.6
15DIA2	15	85	228	77.7	93.6	210	77.9

An evaluation of the effectiveness of the encapsulation with the porous media of the PCMs can be obtained by comparing the enthalpy variation with the amount of PCM present in the mEPCM. If the proportion between the content of PCM and ΔH is respected, then a complete and effective encapsulation has been achieved. The encapsulation coefficient (E_c%) is defined as reported in Equation (1).

$$\text{Encapsulation coefficient}: \; E_c\% = \frac{\Delta H_{mEPCM}}{X_{mEPCM}^{PCM} * \Delta H_{PCM}} \cdot 100 \quad (1)$$

where ΔH_{mEPCM} is the phase change enthalpy of the *mEPCM*, ΔH_{PCM} is the phase change enthalpy of the PCM and X_{mEPCM}^{PCM} is the fraction by weight of nominal PCM in the mEPCM formulation. The E_c% values calculated for the two mEPCMs samples show that the 20DIA2 sample reaches a value close to 100%, which constitutes the complete stabilization of the PCM. By increasing the PCM content, as in 15DIA2, the Ec% value decreases while the absolute enthalpy values of 20DIA2 and 15DIA2 (77.7 and 77.9 J/g) are equivalent; this result leads to the conclusion that the absorption limit of the DIA2 for the PCM is only 80%. The shifts in the temperature of the melting peak can be interpreted concerning the stability of the encapsulation, as a good encapsulation delays the melting, which produces an increasing T_m. Mirroring this, similar results can also be found during cooling. In conclusion, the best encapsulation is obtained with the 20DIA2 sample produced with diatomite and 80% of PCM, which achieves an encapsulation coefficient of 99.7% for the mEPCM.

In Figure 7, the morphological study of the mEPCM also provides important information about the results of the DSC thermal characterization. SEM micrographs contribute to the understanding of the encapsulation dynamics with which the porous medium acts [67,69,72]. By comparing the micrographs of PM alone (DIA2) and mEPCM, it is possible to distinguish the impregnation effect of the salts on absorbent particles. Sample 20DIA2 shows that complete filling of the diatomite cavities with PCMs has been achieved, forming a compact and well-bonded composite surface. Higher quantities of salts cannot be absorbed by this porous medium. From the micrographs of sample 15DIA2, it is possible to note the total covering of the porous medium with an excess of eutectic salts.

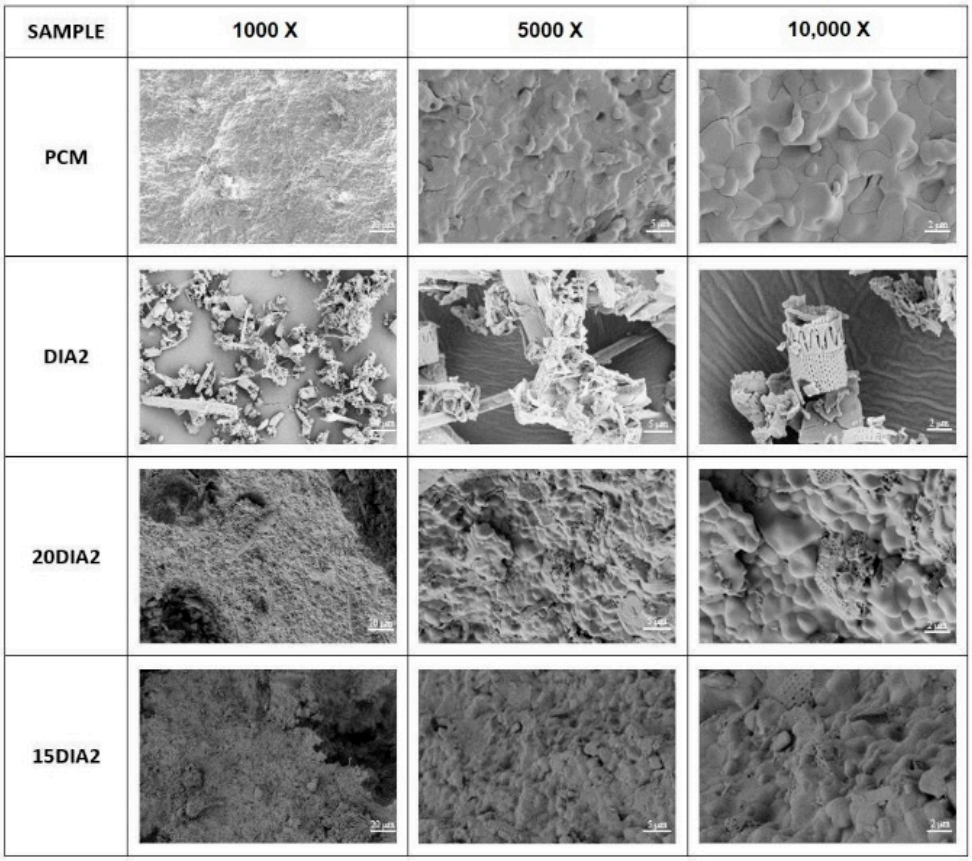

Figure 7. FESEM micrographs of the eutectic PCM, of the diatomite PM (DIA2) and the mEPCM samples with 80% (20DIA2) and 85% (15DIA2) of PCM.

2.2. Base Concrete Mix Design

Based on the experience gained in recent years, as a result of a collaboration between ENEA and Cipiccia Calcestruzzi, a mix design for basic concrete has been developed. It is summarized in Table 3. This mix design shows a low water/cement ratio (w/c) equal to 0.32 and a fresh concrete density of approximately 2434 kg/m^3.

Table 3. Base concrete mix design.

Component	Component Weight in 1 m^3 of Concrete (kg/m^3)
Water	117
Cement	360
Washed sand 0–4 mm	929
Small rubble 5–15 mm	467
Rubble 15–30 mm	504
Metal fibers	50
Synthetic fibers	1
Super-fluidifying	4.32
Volume mass for fresh concrete	2434

The basic mixture of concrete has been designed to be suitable to operate as a heat storage medium at a temperature of at least 400 °C. The presence in the mix design of metal fibers was necessary to promote the thermal conductivity of the material and reduce the charging and discharging times, as well as to increase the mechanical resistance of the material. The nylon fibers, instead, are suitable to limit the probability of spalling phenomena (the more or less violent detachment of sections of material due to the high pressure produced by the vaporization of the free water of the concrete).

The metal fibers used are the Fibercoll M13 (General Admixtures, Treviso, Italy). These are made of steel, cold-drawn, low-carbon and hook-shaped in order to better adhere to the cement matrix. The fibers are 13 mm long and have a diameter of 0.2 mm. The nylon fibers (Meraflex, Cerignola, Italy) were adopted. These are short fibers for polypropylene concrete, with a length of 12.4 mm and a diameter of 0.021 mm. To increase the workability of the materials, a particular super-fluidizer was added, the PRIMIUM HR350 (General Admixtures, Treviso, Italy). This is a polymer-based super-fluidizer that is employed for the production of low water/cement concrete and self-compacting concrete (SCC).

2.3. Concrete/PCM/Diatomite Composites

The mix designs of the concrete containing a nominal percentage by weight of 5% and 10% of PCM had to incorporate about 126 kg and 208 kg, respectively, of mEPCM for each cubic meter of material. These inclusions substitute corresponding volume aggregates (Table 4). These two mix designs show a low water/cement ratio (w/c) equal to 0.37 and 0.41 and a fresh concrete density of approximately 2305 kg/m^3 and 2206 kg/m^3, respectively. The presence of 5.45% and 9.43% of mEPCM makes the new materials lighter than the basic concrete.

Table 4. Concrete/mEPCM mix design.

Component	Component Weight in 1 m^3 of Concrete (kg/m^3)	
	with 5 wt% of mEPCM	with 10 wt% of mEPCM
Water	133	148
Cement	360	360
Washed sand 0–4 mm	853	822
Small rubble 5–15 mm	371	288
Rubble 15–30 mm	407	324
mEPCM	126	208
Metal fibers	50	50
Synthetic fibers	1	1
Super-fluidifying	4.32	4.32
Volume mass for fresh concrete	2305	2206

2.4. Plain Cylindrical Specimen Production

Using the previous three mix designs, the basic concrete and the concrete with the addition of 5 wt% and 10 wt% of PCM, 90 plain cylindrical specimens (30 for each material), to be subjected to thermal and mechanical characterization, were made. These specimens had all the nominal dimensions: 100 mm diameter and 200 mm height. These dimensions were derived from the EN 12390-1 standard [73]. The specimens had a nominal volume of 1.57 dm^3 and a weight of around 3.8 kg. Plain cylindrical specimens were uniquely identified with two letters and a number as follows: an initial letter indicating the type of material (A, for base concrete; B, for concrete with 5 wt% PCM; C, for concrete with 10 wt% PCM); a second letter indicating the type of test for which they were intended (X for thermal and compression tests; Y for an indirect tensile test); a progressive number from 01 to 15. For the production and curing of the specimens, the EN 12390-2 standard [74] was followed. In particular, starting from the studied mix designs, the necessary amounts of all materials required, including water and additives, were recovered, placed in a square shovel-mixing container and carefully mixed. Then, the mixed concrete was placed into appropriate cylindrical molds. During the casting, the concrete was compacted by an internal mechanical vibrator. The samples were left in the molds for around 24 h, protected from shock, vibration and dehydration, at a temperature of 20 $\pm$ 5 °C. Then, once they were removed from the mold, 28 days were expected for complete hardening in a tank at 100% humidity and 15–20 °C.

2.5. Degassing and Thermal Conditioning for Specimens

All the solid cylindrical specimens produced (30 for each series) before thermal and mechanical characterization were subjected to a degassing phase (free water removal) and heat treatment at one of the project's reference temperatures (200, 300 or 400 °C). The procedure for degassing and thermal conditioning of the concrete specimens consisted of three phases:

- Preliminary phase: size measurement and weight;
- Degassing phase: free water removal;
- Thermal conditioning phase: treatment at a set temperature.

The objective of the preliminary phase was to identify and measure the dimensions and weight of the solid cylindrical specimens in agreement with EN 12390-1 [73] and EN 12390-7 [75]. A precision balance (Kern&Sohn, Balingen, Germany, PRJ 6200-2M model) was used for weighing the specimens. The first 3 specimens of each type (18 in total: AXi, AYi, BXi, BYi, CXi, CYi, with i = 01, 02, 03) were selected and wrapped in a transparent "waterproofing" film to avoid the possible reabsorption of the ambient humidity. The other specimens were brought to the degassing phase.

The Sunrise SU340 Climatic Chamber (Angelantoni, Massa Martana, Italy) was used for the degassing phase (Figure 8a). In Figure 8b, the evolutions of the temperature and the relative humidity set in the climate chamber for the degassing session are reported. Afterwards, visual analysis was carried out to detect eventual damage, and a picture was taken of the specimens, which were then wrapped in a waterproofing film. Six specimens were set aside (AXi, AYi, BXi, BYi, CXi, CYi, with i = 04, 05, 06), while the others were subjected to the higher-temperature treatments in the furnace.

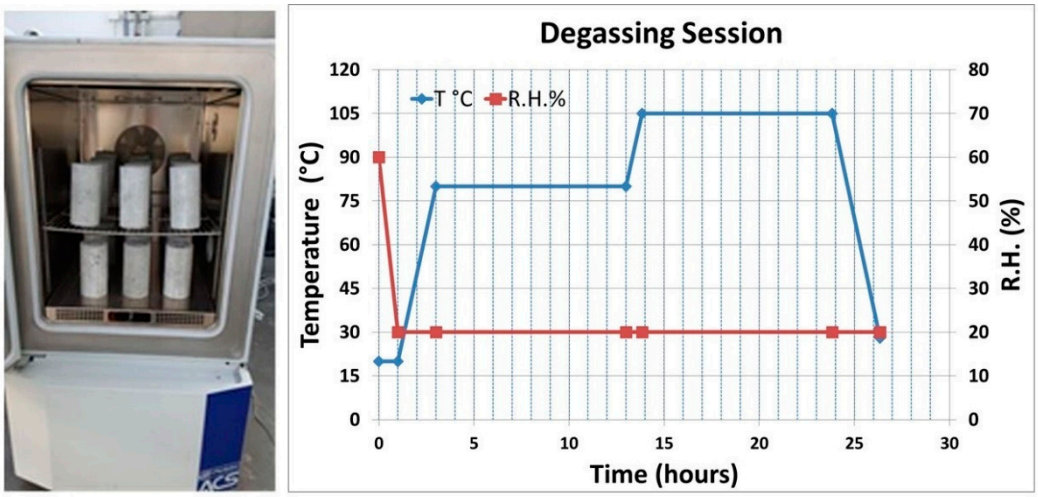

Figure 8. Some specimens inside the climatic chamber ready for the degassing (**a**) and evolution of temperature and humidity in degassing phase (**b**).

In the last phase, the remaining solid cylindrical specimens (18 per type of material) and in groups of 6 were treated at 200, 300 and 400 °C, respectively, using a model LHT-6/120 Carbolite programmable furnace. The assumed set-point temperature varied according to the following steps:

- for the first 3 sets of 6 specimens (AXi, AYi, BXi, BYi, CXi, CYi, with i = 07, 08, 09): ramp up from 50 °C to 200 °C in 2 h, permanence at 200 °C for 10 h and ramp down from 200 °C to 50 °C in 8 h;
- for the second 3 sets of 6 specimens (AXi, AYi, BXi, BYi, CXi, CYi, with i = 10, 11, 12): ramp up from 50 °C to 300 °C in 4 h, permanence at 300 °C for 10 h and ramp down from 300 °C to 50 °C in 10 h;

- for the third 3 sets of 6 specimens (AXi, AYi, BXi, BYi, CXi, CYi, with i = 13, 14, 15): ramp up from 50 °C to 400 °C in 6 h, permanence at 400 °C for 10 h and ramp down from 400 °C to 50 °C in 12 h.

Afterwards, visual analysis was carried out to detect eventual damage, and a picture was taken of the specimens, which were then wrapped in a waterproofing film.

2.6. Thermal and Mechanical Characterization

Thermal characterization of the samples of the new materials was devoted to evaluating their main thermophysical properties, such as density (ρ, (kg/m^3)); thermal conductivity (k, (W(m·°C)); heat capacity (c_p, (J/kg·°C)) and latent heat (λ, (J/kg)). Thus, four essential parameters could be evaluated from them: heat volumic capacity (c_v, (J/m^3·°C)), thermal diffusivity (α, (m^2/s)), thermal effusivity (e, (W/°C·m^2·$\sqrt{s}$)) and best operative thermal range related to the standard use (ΔTo, (K)). Thermal conductivity measurements were carried out using a portable device named ISOMET model 2104 (Applied Precision LTD, Bratislava, Slovakia). Each material was tested four times, and on at least two opposing faces of the cube. Density was measured by the mass and volume rate. Thermal conductivity was detected following the ISO 8301 international standard [76], and specific heat capacity was assessed as a function of the temperature according to the methodology recommended by ISO 11357-1 [77]. Volumetric heat capacity was calculated by Equation (2).

$$c_v = \rho \cdot c_p \tag{2}$$

Thermal diffusivity α (or transmission inertia) is the ratio of thermal conductivity to volumetric heat capacity and is calculated according to Equation (3).

$$\alpha = \frac{k}{\rho \cdot c_p} \tag{3}$$

The thermal effusivity e (or absorption inertia) is assessed by Equation (4).

$$e = \sqrt{k \cdot \rho \cdot c_p} \tag{4}$$

Although diffusivity and effusivity can be assessed by the same physical variables, they measure very different material properties. In fact, materials with high diffusivity transmit fluctuations in the perimeter heat flux more quickly, while those with high effusivity absorb the heat flux from their surface in a better way. For the purposes of the present research, it is worth noting that a good heat capacity combined with low thermal conductivity would determine low thermal diffusivity and high effusivity. Therefore, this material would have a limited activation capacity of the PCM in deeper layers and, consequently, long charge times. On the other hand, a thermal effusivity that is too high would favor the surface heat flux and passive heat exchanges with the internal environment. Therefore, a good balance is needed between the two properties to obtain a material capable of storing high amounts of thermal energy (high e) in a rapid heat transfer process (high α), allowing faster charge and discharge cycles. The values thus measured or calculated were grouped into triples related to the specimens with the same reference or conditioning temperature, and then averaged over time.

The mechanical characterization of the plain cylindrical specimens was performed with two different tests: (i) compressive strength test; (ii) tensile splitting strength test.

The compression strength tests were carried out following the EN 12390-3 standard [78], using a KE series compression machine (Tecnotest, Bergamo, Italy) with a 2000 kN maximum load (Figure 9a). Compressive strength is given by the following equation:

$$f_c = \frac{F}{A_c} \tag{5}$$

where: F is the load at breakage, in N; A_c is the specimen section area on which the compression force acts, calculated from the designated sample measurements, in mm^2; f_c is the compressive strength, in MPa (N/mm^2).

Figure 9. KE series Tecnotest compression machine with maximum load 2000 kN (**a**) and model 3382 Instron traction/compression machine with maximum load 100 kN (**b**).

Indirect tensile strength tests of a plain cylindrical specimen were carried out by applying a compression force to a narrow area, for the entire length of the cylinder. The resulting orthogonal tensile force caused the indirect tensile specimen failure. The cylindrical sample was broken along the plane through the cylinder axis and the contact points of the plates. The equipment used was a model 3382 Instron dynamometer (Instron, Norwood, MA, US) with a 100 kN load cell (Figure 9b) and the EN 12390-6 standard was followed [79]. Indirect tensile strength is given by the following formula:

$$f_{ct} = \frac{2F}{\pi L d} \quad (6)$$

where: f_{ct} is the indirect tensile strength, in MPa or N/mm^2; F is the maximum load, in N; L is the length of the contact line of the specimen, in mm; d is the nominal diameter of the specimen, in mm. The interest in the tensile strength of these materials is due to the negative effect that cracking of concrete has when it is used as a heat storage medium.

3. Results and Discussion

The results of the characterization of the new heat storage materials in terms of density, thermal properties (conductivity, capacity, specific heat, diffusivity and effusivity) and mechanical properties (compression and indirect tensile strength) will be shown and discussed below.

3.1. Weight Loss and Density

The density of the various mix designs was calculated as a weight-to-volume ratio, the latter being estimated as the average value of the three heights and three diameters measured for each concrete specimen. Table 5 shows the average densities for the specimens that were hardened (at 20 °C), degassed (at 105 °C) and heat-conditioned at 200, 300 and 400 °C, respectively. These densities are also compared with the initial ones derived from the formulas of the three mix designs. In Figure 10, the density values and their standard deviation are plotted as a function of the reference temperature.

Table 5. Mix design density for fresh and hardened concrete as a function of heat treatment temperature.

Material Type	Density					
Reference Temperature	**By Formulas**	**20 °C**	**105 °C**	**200 °C**	**300 °C**	**400 °C**
A	2435.0	2378.0	2327.1	2256.7	2245.0	2228.3
Std.dev.	-	25.4	22.9	21.6	16.4	29.3
Weight loss %	2.40%	-	−2.14%	−5.10%	−5.59%	−6.29%
B	2305.0	2373.0	2323.3	2198.3	2198.3	2180.0
Std.dev.	-	17.4	18.1	14.7	27.1	19.0
Weight loss %	−2.87%	-	−2.09%	−7.36%	−7.36%	−8.13%
C	2206.0	2264.7	2202.5	2075.0	2045.0	2030.0
Std.dev.	-	56.5	37.4	28.8	48.9	42.4
Weight loss %	−2.59%	-	−2.75%	−8.38%	−9.70%	−10.36%

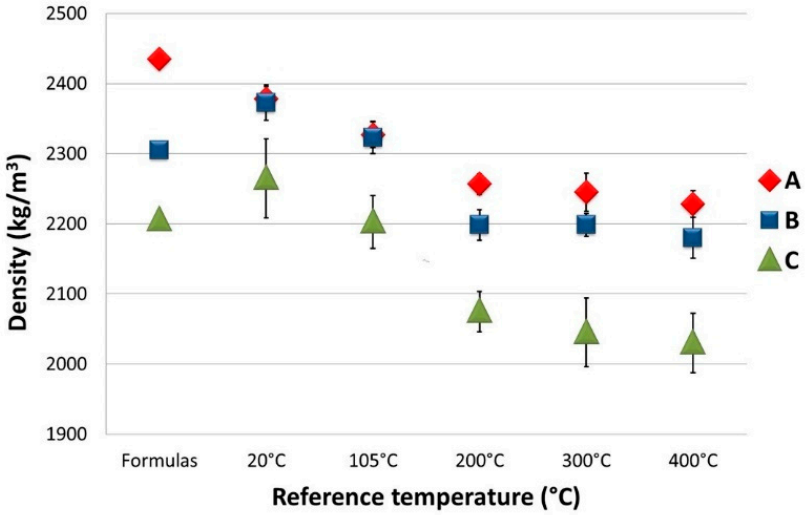

Figure 10. Density of the various mix designs for fresh and hardened concrete as a function of heat treatment temperature.

The density of the type A hardened specimen was around 2.5% lower than that of the formula (2378 kg/m^3). This was due to the loss of free water during the 28 days of curing. After the degassing phase, there was a further 2.1% drop in weight, which was followed by a further 3% decrease after thermal treatment at 200 °C. The latter density value remained constant even after the thermal treatment at 300 °C, highlighting the absence of additional available free water. It decreased again by around 0.7%, after the thermal treatment at 400 °C, where, probably, part of the bonded water started to be extracted. In conclusion, three different zones were identifiable: (i) between 20 and 105 °C, where there was a constant loss of free water; (ii) between 200 and 300 °C, where the free water to be extracted was now very limited; (iii) the one above 400 °C, where part of the bonded water was also extracted, with the consequent onset of material deterioration. Thermal treatment at 105 °C should have extracted most of the free water of the concrete. Instead, after treatment at 200 °C, even more free water was extracted in the previous one. This is an indication that either the degassing temperature should be greater than 105 °C or that the degassing time was too short (currently isotherm for 10 h). Both parameters will probably have to be revised in the future.

Similar behavior could be observed for both the type B (with 5 wt% of mEPCM) and type C (with 10 wt% of mEPCM) specimens. The same three areas of behavior could be identified for these materials too. The only difference was that the hardened concrete and the concrete after degassing showed a density higher than the density calculated by the formula of the mixtures. This anomaly could be caused by abnormal water absorption

during curing (instead of loss). The presence of a great deal of free water was also evidenced by a very important weight loss that occurred after treatment at 200 °C: more than 7% compared to cured specimens of the same type and around 2% compared to type A ones after the same treatment. Type C specimens showed density values much lower than the type B material. This could be an indicator of the presence of free water in a medium with greater porosity. The increased presence of water was also evidenced by the sharp drop in weight that occurred after treatment at 200 °C and continued even after that at 300 °C.

3.2. Mechanical Characterization

The mechanical characterization tests of the specimens gave the results shown in Table 6. They relate to three specimens conditioned at the same reference temperature. As far as the compression tests are concerned, the type of breakage that occurred, as described by the standards, was not well defined since the presence of a large number of metal fibers prevented the specimen from evolving towards one of the classic failure configurations. In Figure 11, the values and standard deviation of the main mechanical results are plotted as a function of the reference temperature.

Table 6. Compression and indirect tensile strength for the concrete mix designs as a function of heat treatment temperature.

Id	T (°C)	f_c (N/mm^2)	f_{ct} (N/mm^2)
A	20	42.63	9.25
A	105	35.72	7.28
A	200	29.62	6.65
A	300	30.26	6.03
A	400	23.25	7.23
B	20	25.39	3.26
B	105	25.39	4.11
B	200	25.39	3.33
B	300	21.02	2.97
B	400	9.89	1.48
C	20	18.05	2.42
C	105	19.09	3.15
C	200	20.74	2.77
C	300	20.08	2.35
C	400	12.49	1.49

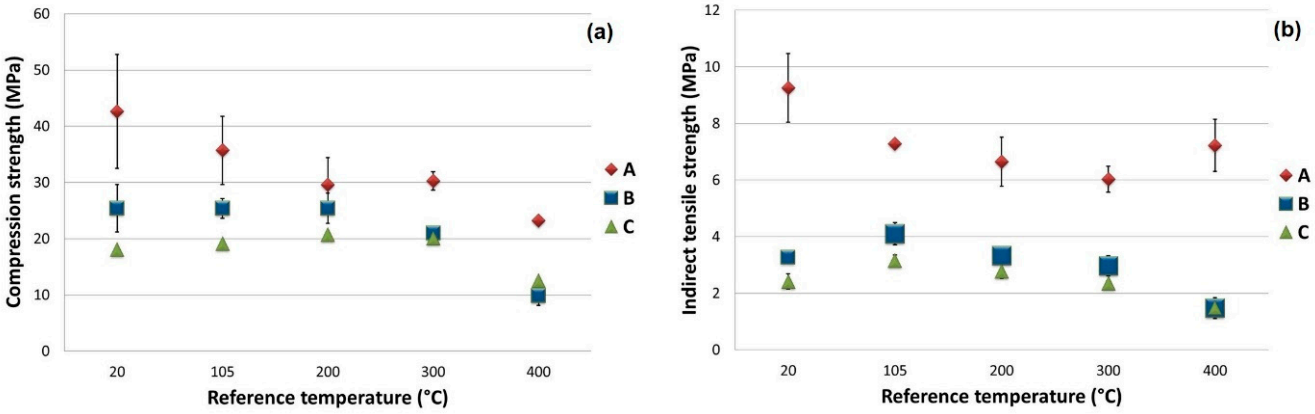

Figure 11. Average compressive (**a**) and indirect traction (**b**) strength, in MPa, for the various concrete mix designs, as a function of the heat treatment temperature.

In type A specimens, f_c compression resistance was, as expected, very high at 20 °C exceeding 40 MPa, due to the high presence of metal fibers. As the treatment temperature

increased, it decreased almost linearly to around 23 MPa. The strong effect of metal fibers was also highlighted by the indirect tensile strength: at 20 °C, the f_{ct} was more than 9 MPa and then reached, at other treatment temperatures, around 7 MPa.

The presence of mEPCM in type B and C specimens greatly reduced the initial compression resistance (25 and 18 MPa at 20 °C, respectively) while remaining almost constant up to treatment temperatures of around 200 °C. Beyond these temperatures, perhaps due to the voids created by the evaporation of free water and the bonded water, the strength was reduced almost linearly to around 22 MPa. A behavior similar to the compression tests was also evident for indirect tensile strength: up to 300 °C, the f_{ct} value was around 3 MPa and, subsequently, it decreased to around 1.5 MPa.

3.3. Thermal Characterization

Table 7 shows the average values of the thermal characterization according to the type of material and the reference temperature. These results are the average of the values associated with three different specimens. These values are, in turn, an average of at least three measurements carried out at different points on the surface of a single specimen.

Table 7. Thermal properties of the concrete mix designs.

Material Type	T_{ref} (°C)	ρ (kg/m^3)	k (W/m·C)	Cv (J/m^3·C)	α (m^2/s)	Cp (J/kg·°C)	e (W/°C·m^2·$\sqrt{s}$)
A	20	2390.00	1.90	$1.45 \cdot 10^6$	$1.31 \cdot 10^{-6}$	605.23	1655.92
A	105	2333.33	1.94	$1.46 \cdot 10^6$	$1.33 \cdot 10^{-6}$	627.08	1683.29
A	200	2250.00	1.69	$1.42 \cdot 10^6$	$1.2 \cdot 10^{-6}$	631.03	1549.26
A	300	2233.33	1.94	$1.47 \cdot 10^6$	$1.32 \cdot 10^{-6}$	659.66	1687.84
A	400	2203.33	1.62	$1.46 \cdot 10^6$	$1.12 \cdot 10^{-6}$	662.61	1624.21
B	20	2336.67	1.98	$1.48 \cdot 10^6$	$1.33 \cdot 10^{-6}$	633.15	1711.75
B	105	2346.67	1.56	$1.49 \cdot 10^6$	$1.05 \cdot 10^{-6}$	634.89	1524.98
B	200	2263.33	1.60	$1.44 \cdot 10^6$	$1.11 \cdot 10^{-6}$	637.61	1520.55
B	300	2256.67	1.44	$1.43 \cdot 10^6$	$1.01 \cdot 10^{-6}$	633.63	1430.98
B	400	2253.33	1.37	$1.43 \cdot 10^6$	$9.62 \cdot 10^{-7}$	633.16	1553.21
C	20	2373.33	1.46	$1.54 \cdot 10^6$	$9.44 \cdot 10^{-7}$	650.31	1498.45
C	105	2333.33	1.57	$1.54 \cdot 10^6$	$1.02 \cdot 10^{-6}$	660.31	1554.57
C	200	2186.67	1.12	$1.6 \cdot 10^6$	$7.0 \cdot 10^{-7}$	731.79	1336.44
C	300	2196.67	1.07	$1.4 \cdot 10^6$	$7.22 \cdot 10^{-7}$	676.58	1260.96
C	400	2176.67	0.96	$1.51 \cdot 10^6$	$6.35 \cdot 10^{-7}$	695.34	1470.81

In Figure 12, the values and standard deviation of the main thermal results are plotted as a function of the reference temperature. The thermal capacity of the type A specimen was substantially constant and equal to around 1.46 MJ/(m^3 °C) but it increased with the amount of added mEPCM (+2% for type B specimens and +5% for type C specimens). The specific heat increased almost linearly with the treatment temperature, rising from 600–650 J/(kg °C) at 20 °C to around 660–690 J/(kg °C) at 400 °C. This is a consequence of the reduced density of the specimens containing mEPCM, caused by the presence of voids previously filled with free water, and the presence of a good amount of PCM.

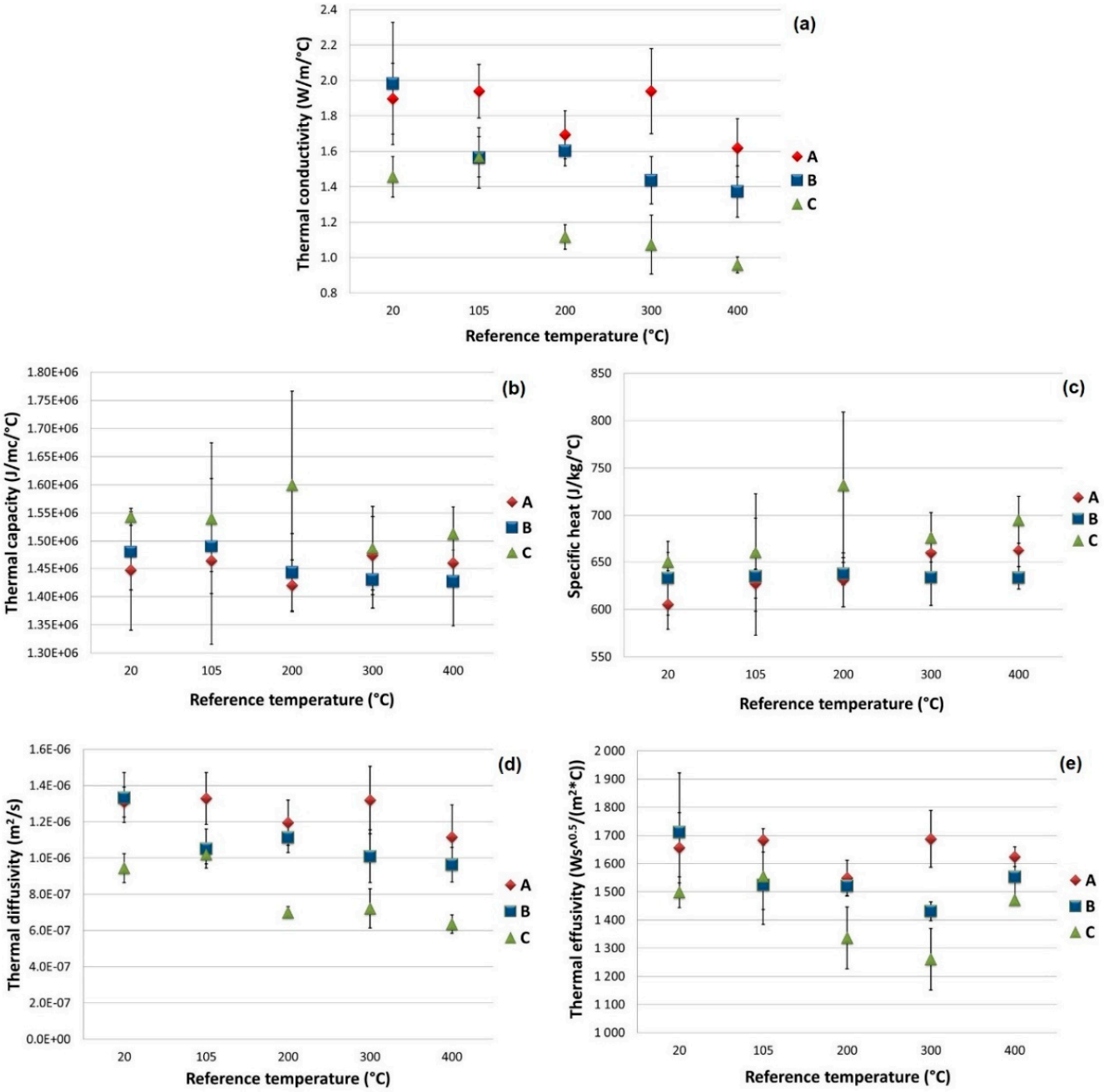

Figure 12. Average thermal properties for the various concrete mix designs, as a function of the heat treatment temperature: conductivity, in W/(m·C) (**a**), capacity, in J/(m^3·C) (**b**), specific heat, in J/(kg·°C) (**c**), diffusivity, in m^2/s (**d**) and effusivity, in (**e**), in (W/°C·m^2·$\sqrt{s}$).

The thermal conductivity of type A and B specimens was in line with the imposed target (2 W/(m °C)), with a value of approximately 1.9 W/(m °C). This value decreased with the increase in the reference temperature, particularly for type B specimens: this behavior was probably due to the cited voids that increased the thermal resistance of the material. This same problem was amplified in type C specimens, where the amount of mEPCM was greater, with the consequence of a strong reduction in thermal conductivity even at low reference temperatures (approximately 1.4 W/(m °C) at 20 °C). The thermal diffusivity and thermal effusivity of the materials closely followed the trend of thermal conductivity.

As could be seen, many of these measures were affected by significant variability. The cause of this lies in the high inhomogeneity of the material and the presence of a high quantity of metal fibers. The used measurement method, which was applied on

limited material surfaces, is particularly affected by this inhomogeneity. To overcome this drawback, a single measurement was repeated and averaged on at least three different zones for each specimen. Despite this, however, a certain variability of the measure itself was evident.

3.4. Discussion

Taking into account any latent heat, the results obtained show that the thermal capacity of the material is greater when there is a greater amount of PCM. Unfortunately, the volume of diatomite used (i.e., the voids connected to its porosity) also increases in mEPCM, implying a clear deterioration in both heat exchange and transmission characteristics, as well as in mechanical ones. As a result, the presence of PCM greater than 10%, in a PCM/diatomite weight ratio of 80/20, is strongly discouraged. The above-mentioned ratio of PCM to diatomite, which, in terms of volume, is 40% of the mEPCM is, unfortunately, a physical limit and therefore difficult to improve. The use of a concrete mix design containing 5% by weight of PCM shows an increase in energy density of approximately 7%, calculated for a thermal variation of 100 °C at an average operating temperature of 250 °C. This increase is certainly a good result, but, of course, it will have to be carefully evaluated in light of an assessment of the mix design costs, associated with the addition of an mEPCM, and therefore its economic sustainability. On the other hand, here too there will be a deterioration, even if more limited, in both the heat exchange and transmission characteristics, as well as in the mechanical ones. It is also clear that the full operation of all these materials is limited to below 400 °C, a temperature at which the thermal and mechanical properties begin to decrease substantially.

The results shown in the present paper are in good agreement with the results of previous studies, even taking into account the differences in materials and sizes. F. Girardi et al. [32] studied a new concrete for TES with the primary aim of improving thermal conductivity. They investigated the use of recycled materials in concrete (e.g., polyamide fibers from post-consumer textile carpet waste, metallic powders or shavings and steel fibers). Their concrete showed high thermal conductivity and was a good candidate for an efficient thermal storage unit. The thermal conductivity of the mix containing polyamide fibers and metallic shavings was 2.74 and 2.13 W/(m °C), before and after thermal treatment of 4 h at 300 °C, respectively. The specific heat was approximately 650–700 J/(kg °C). Moreover, the morphology of this concrete appeared compact and less cracked, even after thermal treatment at a temperature higher than 300 °C. Its compressive strength f_c was 35–40 MPa. These values were mainly obtained through the introduction of a metal charge of around 77 kg per cubic meter of concrete. The effect of the inclusion of PCM particles in concrete, employed as a solid energy storage medium, on its thermal and mechanical behavior was evaluated by Mazzucco et al. [80]. This study was performed through transient thermal analyses of homogenized composite and 3D mechanical finite element (FE) models. It was also developed at the mesoscale level to explicitly represent the main concrete components, such as cement paste, coarse aggregates and steel capsules, with a PCM to better describe the evolutionary process of thermal damage during plant functioning. They referred to a fixed volume fraction (20%) for the inclusions and to vary the solar salt (PCM) filling percentages until admissible, to preserve the thermal capacity of the system and its working conditions. This study showed that the addition of PCM-containing steel capsules has a double effect on the performance of the concrete, depending on the quantity of capsules and their degree of filling: an increase in the stored energy density due to the contribution of latent heat was obtained. Instead, a reduction in thermal conductivity, specific heat and, above all, mechanical strength, were obtained. This last mechanical aspect is due to the damage resulting from the pressure caused by the increase in PCM volume during the phase change. In fact, it has been estimated that with a PCM filling degree of 50%, the concrete begins to damage, with around 70–75% damage values that are no longer bearable by the material. Finally, Chieruzzi et al. [53] attempted to insert 2% by weight of PCM (mEPCM solar salt/diatomite, 80/20) inside a cement mortar consisting of water,

cement and sand. The results obtained showed that the addition of a small amount of phase change material in a cement mortar could lead to positive effects both on the thermal properties (volumetric thermal capacity and conductivity) and on the mechanical ones. The characterization of the material showed that after treatment at 250 °C, there was a weight loss of around 5%, a decrease in thermal conductivity from 1.6 W/(m °C) to around 1.3 W/(m °C) and an increase in energy density of around 10%. The compressive strength was approximately 33 MPa and the flexural strength was 9.8 MPa.

4. Conclusions

The purpose of this work was the development of a new type of heat storage medium based on the use of a widely available, low-cost material, concrete, to which a small amount of phase-changing material, solar salt, was added, microencapsulated in a porous medium, diatomite. In this way, by being able to store energy both as sensible and latent heat, a material with a higher thermal capacity or an increased stored energy density was obtained. Three different types of concrete were made: one without the addition of mEPCM (named A); one including 5% by weight of microencapsulated PCM (named B); one including 10% by weight of microencapsulated PCM (named C). These materials should be able to operate at medium–high temperatures (150–400 °C). Then, they were thermally and mechanically characterized at room temperature after thermal treatment at temperatures between 20 and 400 °C. Characterization of the three mixtures developed led to the following conclusions:

- Three different types of behavior, as a function of treatment temperature, are generally identifiable for the developed material. Below 200 °C, there is still free water in the form of steam in the concrete specimens. This is because the water forms weak dipole bonds with both the porous matrix of the mEPCM and the cement matrix. Between 200 °C and 300 °C, free water has evaporated or continues to evaporate, creating a series of voids inside the material. Finally, above 300 °C, part of the bonded water also begins to be extracted, reducing the grip between cement and aggregates and deteriorating the material.
- All the untreated materials have a density of approximately 2370 kg/m^3 below 105 °C, but this reduces as the treatment temperature increases. Between 200 °C and 300 °C, this reduction ranges from 5% for mix A to over 7% for mixes B and C.
- The thermal capacity of the three mixes increases slightly depending on the amount of the mEPCM present, increasing from approximately 2% of mix B to 5% of mix C, and is inversely proportional to the reduction in density. Therefore, this is expressed in an increase in the specific heat value of materials with more mEPCM: from 610 J/(kg °C) of mix A to 630 J/(kg °C) of mix B and 650 J/(kg °C) of mix C. Specific heat seems to improve by increasing the treatment temperature.
- Thermal conductivity is certainly good for mix A (>1.9 W/(m °C)) even after various heat treatments. Mix B shows a good initial conductivity which, however, is reduced after heat treatments up to around 1.5 W/(m °C). Instead, the conductivity of mix C is well below the previous values, which are between 1.5 and 0.9 W/(m °C). The increase in conductivity values is certainly due to the presence of a good amount of metal fibers, which act as a thermal bridge, while its decrease with temperature is probably due to the voids present in the mEPCM once the free water is removed.
- The other quantities that characterize the exchange and transport capabilities of materials, or thermal diffusivity and effusivity, show a close correlation with thermal conductivity.
- The effect of the presence of metal fibers is evident in terms of the compressive strength and, above all, the tensile strength of all materials. Instead, the presence of mEPCM and, most importantly, the removal of free water from its pores after the various heat treatments characterizes the difference in mechanical performance between mix A and the others.

In summary, by adding a non-excessive amount of microencapsulated material to the mixture (5 wt%), it is possible to improve the energy density by around 7% to avoid

mechanical problems (the formation of cracks) and a consequent decrease in heat transmission. Although this may not appear to be an exceptional improvement, it is important, in absolute terms, for the decrease in storage volumes and land use, which are usually large in CSP systems.

The results of this work demonstrate how the materials developed and characterized in this paper are not only in agreement with what was previously highlighted but also constitute a synthesis of the best characteristics both from a thermal and a mechanical point of view, and can be useful for applications such as CSP/CST, heat production for an industrial process at medium temperature, heating and cooling for districts or buildings, water desalination and heat waste recovery.

Since this analysis was based on room temperature measurements, albeit also including some heat treatments, it would be useful to study the related heat exchange conditions and storage capacity when it is integrated into a tube and shell storage system. This will be the objective of future experimental analyses for the current research line.

Author Contributions: A.M. and R.L. conceived and wrote the paper; F.D. and L.T. studied and synthesized the mEPCM; M.C. studied the concrete mix-design and realized all specimens; A.M. and D.N. designed the experiments; R.L., E.V. and D.N. conducted concrete degassing and thermal condition phases; A.M. and M.C. analyzed the experimental data. All authors have read and agreed to the published version of the manuscript.

Funding: This research was funded by the Italian Ministry of Economic Development through the Research on Electric System—PTR 2019-21—Objective: Technologies—Project 1.2/WP2 (Thermal Storage).

Acknowledgments: The authors also thank G.M. Giannuzzi, who inspired this activity. He provided advice that was essential for the success of this work.

Conflicts of Interest: The authors declare no conflict of interest. The funders had no role in the design of the study; in the collection, analyses, or interpretation of data; in the writing of the manuscript, or in the decision to publish the results.

References

1. OECD. *World Energy Outlook 2018*; OECD/IEA: Paris, France, 2018.
2. EIA. *International Energy Outlook 2019 with Projections to 2050*; U.S. Energy Information Administration, Office of Energy Analysis, U.S. Department of Energy: Washington, DC, USA, 2019; p. 20585.
3. UNFCCC. *Paris Agreement. XXI Conference Parties*; FCCC/CP/2015/L.9/Rev.1; UNFCCC: Paris, France, 2015; p. 32.
4. Sorrell, S. Reducing energy demand: A review of issues, challenges and approaches. *Renew. Sustain. Energy Rev.* **2015**, *47*, 74–82. [CrossRef]
5. Iddrisu, I.; Bhattacharyya, S.C. Sustainable energy development index: A multi-dimensional indicator for measuring sustainable energy development. *Renew. Sustain. Energy Rev.* **2015**, *50*, 513–530. [CrossRef]
6. IRENA. *Scenarios for the Energy Transition: Global Experiences and Best Practices*; International Renewable Energy Agency: Abu Dhabi, United Arab Emirates, 2020; ISBN 978-92-9260-267-3.
7. IRENA. *Renewable Power Generation Costs in 2019*; International Renewable Energy Agency: Abu Dhabi, United Arab Emirates, 2020; ISBN 978-92-9260-244-4.
8. ELREN. *Renewable Energy Training Manual*; Carlow LEADER and Tipperary Institute: Carlow, Ireland, 2007.
9. CSP Alliance. The Economic and Reliability Benefits of CSP with Thermal Energy Storage. Available online: http://www.brightsourceenergy.com (accessed on 23 January 2021).
10. Jacob, R.; Belusko, M.; Liu, M.; Saman, W.; Bruno, F. Using renewables coupled with thermal energy storage to reduce natural gas consumption in higher temperature commercial/industrial applications. *Renew. Energy* **2019**, *131*, 1035–1046. [CrossRef]
11. Sarbu, I.; Sebarchievici, C. A Comprehensive Review of Thermal Energy Storage. *Sustainability* **2018**, *10*, 191. [CrossRef]
12. Gajendiran, M.; Nallusamy, N. Application of solar thermal energy storage for industrial process heating. *Adv. Mater. Res.* **2014**, *984–985*, 725–729. [CrossRef]
13. Zhang, H.; Bayens, J.; Cáceres, G.; Degrève, J.; Lv, Y. Thermal energy storage: Recent developments and practical aspects. *Prog. Energy Combust. Sci.* **2016**, *53*, 1–40. [CrossRef]
14. Liu, M.; Saman, W.; Bruno, F. Review on storage materials and thermal performance enhancement techniques for high temperature phase change thermal storage systems. *Renew. Sustain. Energy Rev.* **2012**, *16*, 2118–2132. [CrossRef]
15. Gibb, D.; Johnson, M.; Romaní, J.; Gasia, J.; Cabeza, L.F.; Seitz, A. Process integration of thermal energy storage systems—Evaluation methodology and case studies. *Appl. Energy* **2018**, *230*, 750–760. [CrossRef]

16. Romaní, J.; Gasia, J.; Solé, A.; Takasu, H.; Kato, Y.; Cabeza, L.F. Evaluation of energy density as performance indicator for thermal energy storage at material and system levels. *Appl. Energy* **2019**, *235*, 954–962. [CrossRef]
17. Emerson, J.; Micah, H.; Panneer, S. Concrete as a thermal energy storage medium for thermocline solar energy storage systems. *Sol. Energy* **2013**, *96*, 194–204.
18. Buscemi, A.; Panno, D.; Ciulla, G.; Beccali, M.; Lo Brano, V. Concrete thermal energy storage for linear Fresnel collectors: Exploiting the South Mediterranean's solar potential for agri-food processes. *Energy Convers. Manag.* **2018**, *166*, 719–734. [CrossRef]
19. Tamme, R.; Laing, D.; Steinmann, W.D. Advanced Thermal Energy Storage Technology for Parabolic Trough. *J. Sol. Energy Eng.* **2004**, *126*, 794–800. [CrossRef]
20. Salomoni, V.A.; Majorana, C.E.; Giannuzzi, G.M.; Miliozzi, A.; Di Maggio, R.; Girardi, F.; Mele, D.; Lucentini, M. Thermal storage of sensible heat using concrete modules in solar power plants. *Sol. Energy* **2014**, *103*, 303–315. [CrossRef]
21. Bataineh, K.; Gharaibeh, A. Optimal design for sensible thermal energy storage tank using natural solid materials for a parabolic trough power plant. *Sol. Energy* **2018**, *171*, 519–525. [CrossRef]
22. Laing, D.; Steinmann, W.D.; Tamme, R. Solid media thermal storage for parabolic trough power plants. *Sol. Energy* **2006**, *80*, 1283–1289. [CrossRef]
23. Laing, D.; Lehmann, D.; Fiß, M.; Bahl, C. Test Results of Concrete Thermal Energy Storage for Parabolic Trough Power Plants. *J. Sol. Energy Eng.* **2009**, *131*, 041007. [CrossRef]
24. Laing, D.; Bauer, T.; Lehmann, D.; Bahl, C. Development of a Thermal Energy Storage System for Parabolic Trough Power Plants With Direct Steam Generation. *J. Sol. Energy Eng.* **2010**, *132*, 021011. [CrossRef]
25. Martins, M.; Villalobos, U.; Delclos, T.; Armstrong, P.; Bergan, P.G.; Calvet, N. New concentrating solar power facility for testing high temperature concrete thermal energy storage. *Energy Procedia* **2015**, *75*, 2144–2149. [CrossRef]
26. Hoivika, N.; Greiner, C.; Barragan, J.; Iniesta, A.C.; Skeie, G.; Bergan, P.; Blanco-Rodriguez, P.; Calvet, N. Long-term performance results of concrete-based modular thermal energy storage system. *J. Energy Storage* **2019**, *24*, 100735. [CrossRef]
27. Skinner, J.E.; Strasser, M.N.; Brown, B.M.; Selvam, R.P. Testing of High Performance Concrete As A Thermal Energy Storage Medium At High Temperatures. *J. Sol. Energy Eng.* **2014**, *136*, 021004. [CrossRef]
28. Guerrero, L.; Collares Pereira, M. New materials for thermal energy storage in concentrated solar power plants. In Proceedings of the SOLARPACES 2015, Cape Town, South Africa, 13–16 October 2015; Volume 1734, p. 050018.
29. Miliozzi, A.; Giannuzzi, G.M.; Mazzei, D.; Liberatore, R.; Crescenzi, T.; Mele, D. Concrete Based Thermal Energy Storage Devise. Patent 102017000129902, 14 November 2017.
30. Giannuzzi, G.M.; Ozger, O.B.; Girardi, F.; Salomoni, V.A.; Majorana, C.E.; Fambri, L.; Baldassino, N.; Di Maggio, R. Effect of nylon fibres on mechanical and thermal properties of hardened concrete for energy storage systems. *Mater. Des.* **2013**, *51*, 989–997.
31. Giannuzzi, G.M.; Liberatore, R.; Mele, D.; Mazzucco, G.; Xotta, G.; Salomoni, V.A.; Majorana, C.E.; Di Maggio, R. Experimental campaign and numerical analyses of thermal storage concrete modules. *Sol. Energy* **2017**, *157*, 596–602. [CrossRef]
32. Giannuzzi, G.M.; Girardi, F.; Mazzei, D.; Salomoni, V.A.; Majorana, C.E.; Di Maggio, R. Recycled additions for improving the thermal conductivity of concrete in preparing energy storage systems. *Constr. Build. Mater.* **2017**, *135*, 565–579.
33. Nomura, T.; Okinaka, N.; Akiyama, T. Impregnation of porous material with phase change material for thermal energy storage. *Mater. Chem. Phys.* **2009**, *115*, 846–850. [CrossRef]
34. De Gracia, A.; Cabeza, L.F. Phase change materials and thermal energy storage for buildings. *Energy Build.* **2015**, *103*, 414–419. [CrossRef]
35. Memon, S.A. Phase change materials integrated in building walls: A state of the art review. *Renew. Sustain. Energy Rev.* **2014**, *31*, 870–906. [CrossRef]
36. Umair, M.M.; Zhang, Y.; Iqbal, K.; Zhang, S.; Tang, B. Novel strategies and supporting materials applied to shape-stabilize organic phase change materials for thermal energy storage—A review. *Appl. Energy* **2019**, *235*, 846–873. [CrossRef]
37. Karlsson, J. Possibilities of Using Thermal Mass in Buildings to Save Energy, Cut Power Consumption Peaks and Increase the Thermal Comfort. Licentiate Thesis, Lund University, Lund, Schweden, 2012.
38. Ndiaye, K.; Ginestet, S.; Cyr, M. Thermal energy storage based on cementitious materials: A review. *Energy* **2018**, *6*, 97–120. [CrossRef]
39. Pomianowski, M.; Heiselberg, P.; Jensen, R.L. Dynamic heat storage and cooling capacity of a concrete deck with PCM and thermally activated building system. *Energy Build.* **2012**, *53*, 96–107. [CrossRef]
40. Eddhahak-Ouni, A.; Drissi, S.; Colin, J.; Neji, J.; Care, S. Experimental and multi-scale analysis of the thermal properties of Portland cement concretes embedded with microencapsulated Phase Change Materials (PCMs). *Appl. Therm. Eng.* **2014**, *64*, 32–39. [CrossRef]
41. Pisello, A.L.; D'Alessandro, A.; Fabiani, C.; Fiorelli, A.P.; Ubertini, F.; Cabeza, L.F.; Materazzi, A.L.; Cotana, F. Multifunctional analysis of innovative PCM-filled concretes. *Energy Procedia* **2017**, *111*, 81–90. [CrossRef]
42. Pisello, A.L.; Fabiani, C.; Cotana, F. New experimental technique to investigate the thermal behavior of PCM/doped concrete for enhancing thermal/energy storage capability of building envelope. *Energy Procedia* **2017**, *126*, 139–146. [CrossRef]
43. Olivieri, L.; Tenorio, J.A.; Revuelta, D.; Navarro, L.; Cabeza, L.F. Developing a PCM-enhanced mortar for thermally active precast walls. *Constr. Build. Mater.* **2018**, *181*, 638–649. [CrossRef]

44. Sarıa, A.; Bicer, A.; Karaipekli, A.; Al-Sulaiman, F.A. Preparation, characterization and thermal regulation performance of cement based-composite phase change material. *Sol. Energy Mater. Sol. Cells* **2018**, *174*, 523–529. [CrossRef]
45. Drissi, S.; Ling, T.C.; Mo, K.H. Thermal performance of a solar energy storage concrete panel incorporating phase change material aggregates developed for thermal regulation in buildings. *Renew. Energy* **2020**, *160*, 817–829. [CrossRef]
46. Qian, T.T.; Li, J.H.; Min, X.; Deng, Y.; Guan, W.M.; Ning, L. Diatomite: A promising natural candidate as carrier material for low, middle and high temperature phase change material. *Energy Convers. Manag.* **2015**, *98*, 34–45. [CrossRef]
47. Guan, W.M.; Li, J.H.; Qian, T.T.; Wang, X.; Deng, Y. Preparation of paraffin/expanded vermiculite with enhanced thermal conductivity by implanting network carbon in vermiculite layers. *Chem. Eng. J.* **2015**, *277*, 56–63. [CrossRef]
48. Zhang, Z.G.; Zhang, N.; Peng, J.; Fang, X.M.; Gao, X.N.; Fang, Y.T. Preparation and thermal energy storage properties of paraffin/expanded graphite composite phase change material. *Appl. Energy* **2012**, *91*, 426–431. [CrossRef]
49. Gao, H.; Wang, J.; Chen, X.; Wang, G.; Huang, X.; Li, A.; Dong, W. Nano-confinement effects on thermal properties of nano-porous shape-stabilized composite PCMs: A review. *Nano Energy* **2018**, *53*, 769–797. [CrossRef]
50. Voronin, D.V.; Ivanov, E.; Gushchin, P.; Fakhrullin, R.; Vinokurovm, V. Clay Composites for Thermal Energy Storage: A Review. *Molecules* **2020**, *25*, 1504. [CrossRef] [PubMed]
51. Mastroleo, M. Design and Formulation of Materials for Energy Storage Applications. Master's Thesis, Polytechnic of Turin, Turin, Italy, 15 March 2020.
52. Cárdenas, B.; León, N. High temperature latent heat thermal energy storage: Phase change materials, design considerations and performance enhancement techniques. *Renew. Sustain. Energy Rev.* **2013**, *27*, 724–737. [CrossRef]
53. Miliozzi, A.; Chieruzzi, M.; Torre, L. Experimental investigation of a cementitious heat storage medium incorporating a solar salt/diatomite composite phase change material. *Appl. Energy* **2019**, *250*, 1023–1035. [CrossRef]
54. Kramer, C.M.; Wilson, C.J. The phase diagram of $NaNO_3$-KNO_3. *Thermochim. Acta* **1980**, *42*, 253–264. [CrossRef]
55. Benages-Vilau, R.; Calvet, T.; Cuevas-Diarte, M.A.; Oonk, H.A.J. The $NaNO_3$–KNO_3 phase diagram. *Phase Transit.* **2016**, *89*, 1–20. [CrossRef]
56. D'Aguanno, B.; Karthik, M.; Grace, A.N.; Floris, A. Thermostatic properties of nitrate molten salts and their solar and eutectic mixtures. *Sci. Rep.* **2018**, *8*, 10485. [CrossRef]
57. Zhaoa, Q.G.; Hu, C.X.; Liu, S.J.; Guo, H.; Wu, Y.T. The thermal conductivity of molten $NaNO_3$, KNO_3, and their mixtures. *Energy Procedia* **2017**, *143*, 774–779. [CrossRef]
58. Fernández, A.G.; Gomez-Vidal, J.; Oró, E.; Kruizenga, A.; Solé, A.; Cabeza, L.F. Mainstreaming commercial CSP systems: A technology review. *Renew. Energy* **2019**, *140*, 152–176. [CrossRef]
59. Pfleger, N.; Bauer, T.; Martin, C.; Eck, M.; Wörner, A. Thermal energy storage—Overview and specific insight into nitrate salts for sensible and latent heat storage. *Beilstein J. Nanotechnol.* **2015**, *6*, 1487–1497. [CrossRef]
60. Yin, X.; Yu, X.; Wu, X.; Fu, X.; Wu, H.; Zeng, D. Solubility Prediction and Measurement of the System KNO3–LiNO3–NaNO3–H2O. *J. Chem. Eng. Data* **2013**, *58*, 1839–1844. [CrossRef]
61. Elden, H.; Morsy, G.; Bakr, M. Diatomite: Its Characterization, Modifications and Applications. *Asian J. Mater. Sci.* **2010**, *2*, 121–136.
62. Hadjar, H.; Hamdi, B.; Jaber, M.; Brendlé, J.; Kessaıssia, Z.; Balard, H.; Donnet, J.B. Elaboration and characterisation of new mesoporous materials from diatomite and charcoal. *Microporous Mesoporous Mater.* **2008**, *107*, 219–226. [CrossRef]
63. Lutynski, M.; Sakiewicz, P.; Lutynska, S. Characterization of Diatomaceous Earth and Halloysite Resources of Poland. *Minerals* **2019**, *9*, 670. [CrossRef]
64. Meradi, H.; Atouib, L.; Bahloul, L.; Boubendira, K.; Bouazdia, A.; Ismail, F. Characterization by thermal analysis of natural kieselguhr and sand for industrial application. *Energy Procedia* **2015**, *74*, 1282–1288. [CrossRef]
65. Şan, O.; Gören, R.; Özgür, C. Purification of diatomite powder by acid leaching for use in fabrication of porous ceramics. *Int. J. Miner. Process.* **2009**, *93*, 6–10. [CrossRef]
66. Deref, S.p.A.—Castiglione in Teverina. Available online: https://deref-spa-castiglione-in-teverina.business.site/ (accessed on 9 February 2021).
67. Ibrahim, S.S.; Selim, A.Q. Heat treatment of natural diatomite. *Physicochem. Probl. Miner. Process* **2012**, *48*, 413–424.
68. Deng, Y.; Li, J.; Qian, T.; Guan, W.; Wang, X. Preparation and Characterization of KNO3/Diatomite Shape-Stabilized Composite Phase Change Material for High Temperature Thermal Energy Storage. *J. Mater. Sci. Technol.* **2017**, *33*, 198–203. [CrossRef]
69. Lenga, G.; Qiao, G.; Jiang, Z.; Xu, G.; Qin, Y.; Chang, C.; Ding, Y. Micro encapsulated & form-stable phase change materials for high temperature thermal energy storage. *Appl. Energy* **2018**, *217*, 212–220.
70. Chieruzzi, M.; Cerritelli, G.F.; Miliozzi, A.; Kenny, J.M. Effect of nanoparticles on heat capacity of nanofluids based on molten salts as PCM for thermal energy storage. *Nanoscale Res. Lett.* **2013**, *8*, 448. [CrossRef]
71. Jeong, S.G.; Jeon, J.; Lee, J.H.; Kim, S. Optimal preparation of PCM/diatomite composites for enhancing thermal properties. *Int. J. Heat Mass Transf.* **2013**, *62*, 711–717. [CrossRef]
72. Li, X.; Sanjayan, J.G.; Wilson, J.L. Fabrication and stability of form-stable diatomite/paraffin phasechange material composites. *Energy Build.* **2014**, *76*, 284–294. [CrossRef]
73. Testing Hardened Concrete. *Part 1: Shape, Dimensions and Other Requirements for Specimens and Formwork—EN 12390-1*; UNI: Rome, Italy, 2020.
74. Testing Hardened Concrete. *Part 2: Making and Curing Specimens for Strength Tests—EN 12390-2*; UNI: Rome, Italy, 2020.

75. Testing Hardened Concrete. *Part 7: Density of the Hardened Concrete—EN 12390-7*; UNI: Rome, Italy, 2020.
76. ISO. ISO 8301:1991—Thermal insulation—Determination of Steady-State Thermal Resistance and Related Properties—Heat Flow Meter Apparatus. Available online: https://www.iso.org/standard/15421.html (accessed on 12 February 2020).
77. ISO. ISO 11357-1:2016—Plastics—Differential Scanning Calorimetry (DSC)—Part 1: General Principles. Available online: https://www.iso.org/standard/70024.html (accessed on 20 June 2020).
78. Testing Hardened Concrete. *Part 3: Compressive Strength of Test Specimens—EN 12390-3*; UNI: Rome, Italy, 2020.
79. Testing Hardened Concrete. *Part 6: Tensile Splitting Strength of Test Specimens—EN 12390-6*; UNI: Rome, Italy, 2020.
80. Mazzucco, G.; Xotta, G.; Salomoni, V.A.; Giannuzzi, M.; Maiorana, C.E. Solid thermal storage with PCM materials. Numerical investigations. *Appl. Therm. Eng.* **2017**, *124*, 545–559. [CrossRef]